[19] H. Zhang, Y. Liu, and M. Tao, "Resource allocation with subcarrier pairing in OFDMA two-way relay networks," *IEEE Wireless Commun. Lett.*, vol. 1, no. 2, pp. 61–64, Apr. 2012.
[20] M. Peng, Z. Zhao, X. Xie, and W. Wang, "A network coded interference coordination scheme in cellular relay systems," *IEEE Commun. Lett.*, vol. 16, no. 5, pp. 688–690, May 2012.
[21] Y. Jiang, M. Varanasi, and J. Li, "Performance analysis of ZF and MMSE equalizers for MIMO systems: An in-depth study of the high SNR regime," *IEEE Trans. Inf. Theory*, vol. 57, no. 4, pp. 2008–2026, Apr. 2011.
[22] X. Zhang and S. Y. Kung, "Capacity analysis for parallel and sequential MIMO equalizers," *IEEE Trans. Signal Process.*, vol. 51, no. 11, pp. 2989–3002, Nov. 2003.
[23] H. Khun, "The Hungarian method for the assignment problems," *Naval Res. Logist. Quart.*, vol. 2, no. 1/2, pp. 83–97, 1955.
[24] S. Boyd and L. Vandenberghe, *Convex Optimization*. Cambridge, U.K.: Cambridge Univ. Press, 2004.
[25] S. Boyd and A. Mutapcic, "Subgradient methods," Standford Univ., Stanford, CA, USA, Winter 2006, notes for EE364.
[26] W. Yu and R. Lui, "Dual method for nonconvex specturm optimization of multicarrier systems," *IEEE Trans. Commun.*, vol. 54, no. 7, pp. 1310–1322, Jul. 2006.

On Hybrid Overlay–Underlay Dynamic Spectrum Access: Double-Threshold Energy Detection and Markov Model

Xueyuan Jiang, *Student Member, IEEE*,
Kai-Kit Wong, *Senior Member, IEEE*,
Yangyang Zhang, *Member, IEEE*, and
David Edwards, *Senior Member, IEEE*

***Abstract*—In this correspondence, we propose a hybrid strategy that combines overlay and underlay dynamic spectrum access (DSA) schemes. Utilizing a double-threshold energy detection method, unlicensed or secondary users (SUs) can switch between full- and partial-access modes dynamically. A Markov chain model is developed to derive performance metrics for evaluating the proposed strategy. Numerical results show that the proposed strategy can greatly improve the system interfering probability performance. In addition, SUs can adjust the access probability of partial-access mode to tradeoff between throughput and interfering probability performance.**

***Index Terms*—Cognitive radio (CR), double-threshold energy detection, dynamic spectrum access (DSA), hybrid access.**

Manuscript received June 13, 2012; revised October 12, 2012 and February 25, 2013; accepted April 7, 2013. Date of publication April 16, 2013; date of current version October 12, 2013. This work was supported in part by the Guangdong Science and Technology Plan Project under Grant 2011A010801009, by the Shenzhen Science and Technology Plan Project under Grant JC201005280649A, by the Guangdong High-End Electronic Information Special in Strategic Emerging Industry Development Plan under Grant 2012556019, and by the Introduction of Innovative R&D Team Program of Guangdong Province under Grant 2009010005. The review of this paper was coordinated by Dr. H. Jiang.

X. Jiang and D. Edwards are with the Department of Engineering Science, University of Oxford, Oxford OX1 3PJ, U.K. (e-mail: xueyuan.jiang@eng.ox.ac.uk; david.edwards@eng.ox.ac.uk).

K.-K. Wong is with the Department of Electronic and Electrical Engineering, University College London, London WC1E 7JE, U.K. (e-mail: kai-kit.wong@ucl.ac.uk).

Y. Zhang is with the Shenzhen Key Laboratory of Artificial Microstructure Design and the Guangdong Key Laboratory of Meta-RF Microwave Radio Frequency, Kuang-Chi Institute of Advanced Technology, Shenzhen 518000, China (e-mail: yangyang.zhang@kuang-chi.org).

Color versions of one or more of the figures in this paper are available online at http://ieeexplore.ieee.org.

Digital Object Identifier 10.1109/TVT.2013.2258360

I. Introduction

Dynamic spectrum access (DSA) [1] and cognitive radio (CR) [2] have been proposed and become the enabling technologies to more intelligently allocate the spectrum to users. Under the framework of DSA, unlicensed or secondary users (SUs) can share the spectrum with licensed or primary users (PUs). With CR capabilities, SUs are able to observe the spectrum activity and dynamically adjust their operating parameters to access vacant spectrum spaces while making sure that no harmful interference is caused to the PUs.

Hierarchical overlay and underlay access schemes have been shown to achieve a good tradeoff between spectrum efficiency and interference control for DSA [1]. For overlay access, SUs perform spectrum sensing to obtain the current spectrum occupancy information and access the spectrum not used by PUs opportunistically. Reliable spectrum sensing algorithms and an optimal sensing–access mechanism have been widely addressed in [3]–[5]. For underlay access schemes, by constraining the transmission power of SUs and minimizing interference to PUs, SUs can access the spectrum even if PUs are active. Efficient power allocation and adaptive interference threshold constraint methods have been presented in [6], [7].

Interference tolerance of PUs is ignored for overlay access, whereas the possibility for SUs to transmit at higher power when PUs are inactive is forbidden for underlay access. Therefore, mixed or hybrid strategies are preferred to improve spectrum efficiency. In [8], a hybrid CR system was proposed, where the system is normally working in overlay mode but may switch to underlay mode based on a probabilistic control method for the departure rate of SU transmitters. In addition, Chakravarthy *et al.* [9] designed a hybrid overlay–underlay waveform to enable a soft decision in CR and to exploit both unused and underused spectrum resources. Later, Khoshkholgh *et al.* [10] further considered the interference- or power-constrained spectrum sharing system and proposed a mixed access strategy in which SUs attempt to transmit with a predefined probability to ensure the overall interference under a certain threshold.

In this correspondence, we propose a hybrid full–partial access strategy for DSA. A double-threshold energy detection method is proposed to identify the PU's operating location. Based on observations, SUs dynamically switch between full- and partial-access modes. A Markov chain model is developed to analyze the proposed strategy. Performance metrics such as the throughput of SUs and interfering probability to PU will be derived. Our main contribution is that we jointly model and analyze spectrum sensing in the physical (PHY) layer with hybrid access in the multiple-access control (MAC) layer.

II. System Model

A. Network Model

We consider a DSA network consisting of N primary channels and a number of PUs and SUs. To make our analysis tractable, we focus on a single primary channel with bandwidth W. Our objective is to study the achievable throughput and the average interfering probability on this channel by introducing the SUs. In particular, there is a pair of SU transmitter (Tx) and receiver (Rx) in a given area of interest. From the SU's viewpoint, a PU transmitter (Tx) and receiver (Rx) may appear at random locations in the area with radius D_1, as shown in Fig. 1. We also specify the shaded region within radius D_2 as Region 2 in the figure, and its operational meaning will be explained later. We assume that a PU can be referred to as a pair of PU Tx and Rx, which are located in the same region (Region 1 or Region 2), but their locations are independent and randomly distributed within that region.

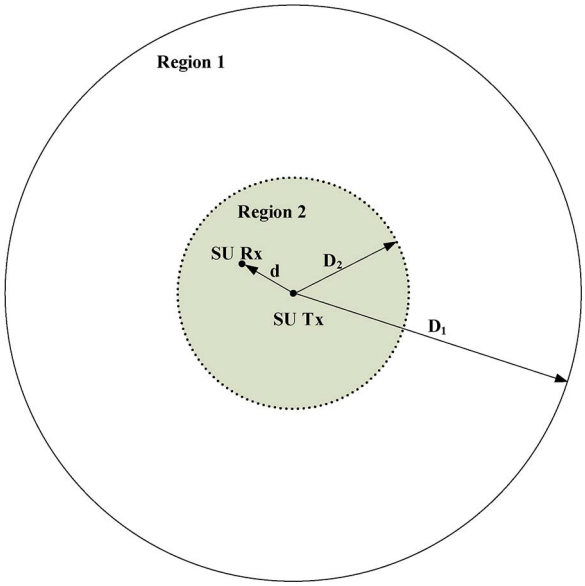

Fig. 1. DSA system model with hybrid access strategy.

It is assumed that the PU and the SU transmit at fixed power levels P_{PU}^t and P_{SU}^t, respectively.

B. Proposed Hybrid Access Strategy

The received energy level over the channel with bandwidth W during sensing time T_s is measured by an SU. For Rayleigh fading, the false alarm and detection probabilities are, respectively, given by [3]

$$\mathcal{Q}(v) = \Pr\{Y > v|H_0\} = \frac{\Gamma\left(u, \frac{v}{2}\right)}{\Gamma(u)} \tag{1}$$

$$\begin{aligned}\mathcal{O}(v,\overline{\gamma}) &= \Pr\{Y > v|H_1\} \\ &= e^{-\frac{v}{2}} \sum_{k=0}^{u-2} \frac{1}{k!}\left(\frac{v}{2}\right)^k + \left(\frac{1+\overline{\gamma}}{\overline{\gamma}}\right) \\ &\quad \times \left(e^{-\frac{v}{2(1+\overline{\gamma})}} - e^{-\frac{v}{2}} \sum_{k=0}^{u-2} \frac{1}{k!}\left(\frac{v\overline{\gamma}}{2(1+\overline{\gamma})}\right)^k\right)\end{aligned} \tag{2}$$

where H_0 and H_1 denote the hypothesis that a PU is inactive and active in the channel, respectively; Y is the decision statistics; v is the threshold for energy detection to indicate a positive; $\overline{\gamma}$ is the average received signal-to-noise ratio (SNR) at the SU Rx; and $u = T_s W$ is the time–bandwidth product. In addition, $\Gamma(\cdot)$ and $\Gamma(\cdot,\cdot)$ are the complete and incomplete gamma functions, respectively.

When the PU Tx is near the SU Tx (i.e., PU Tx in Region 2), the average received SNR at the SU Tx is high, and hence, the PU detection probability will be much greater than the case when the PU Tx appears in Region 1. Moreover, if a miss-detection event happens when the PU Tx is in Region 2, it is more likely that the SU's power will violate the interference constraints of the PU. In our proposed hybrid access strategy, a double-threshold energy detection method is therefore used to identify the operating location of the PU Tx and Rx (Region 1 or Region 2). Based on the identification, the SU may switch between full- and partial-access modes.

In the considered scenario, i.e., double-threshold energy detection method, v_{L} and v_{H} are used to identify the operating location of the PU Tx. As a result, the following three-hypothesis testing is established:

$$H_0 : \text{PU is inactive in the channel.} \tag{3a}$$

$$H_1 : \text{PU is active and transmitting in Region 1.} \tag{3b}$$

$$H_2 : \text{PU is active and transmitting in Region 2.} \tag{3c}$$

When time–bandwidth product u is unchanged, we define the following probabilities:

$$P_0(\mathrm{H}) = \Pr\{Y > v_{\mathrm{H}}|H_0\} = \mathcal{Q}(v_{\mathrm{H}}) \tag{4a}$$

$$P_0(\mathrm{L}) = \Pr\{v_{\mathrm{L}} < Y \le v_{\mathrm{H}}|H_0\} = \mathcal{Q}(v_{\mathrm{L}}) - P_0(\mathrm{H}) \tag{4b}$$

$$P_1(\mathrm{H}) = \Pr\{Y > v_{\mathrm{H}}|H_1\} = \mathcal{O}(v_{\mathrm{H}}, \overline{\gamma}_{\mathrm{L}}) \tag{4c}$$

$$P_1(\mathrm{L}) = \Pr\{v_{\mathrm{L}} < Y \le v_{\mathrm{H}}|H_1\} = \mathcal{O}(v_{\mathrm{L}}, \overline{\gamma}_{\mathrm{L}}) - P_1(\mathrm{H}) \tag{4d}$$

$$P_2(\mathrm{H}) = \Pr\{Y > v_{\mathrm{H}}|H_2\} = \mathcal{O}(v_{\mathrm{H}}, \overline{\gamma}_{\mathrm{H}}) \tag{4e}$$

$$P_2(\mathrm{L}) = \Pr\{v_{\mathrm{L}} < Y \le v_{\mathrm{H}}|H_2\} = \mathcal{O}(v_{\mathrm{L}}, \overline{\gamma}_{\mathrm{H}}) - P_2(\mathrm{H}) \tag{4f}$$

where $\overline{\gamma}_{\mathsf{L}}$ and $\overline{\gamma}_{\mathsf{H}}$ denote the average received SNR when the PU Tx is operating in Region 1 and Region 2, respectively. As a consequence, when the measured energy level in the channel is lower than v_{L}, the SU is operating in full-access mode, i.e., can access the channel with probability 1. If the energy level exceeds v_{L} but is lower than v_{H}, then the SU operates in partial-access mode, i.e., can access the channel with probability P_{access}. Otherwise, the SU should stop transmitting and stay inactive in this channel.

The spectrum sensing interval is defined as the time slot between two consecutive spectrum observations. To achieve the tradeoff between SU throughput and interference of PU, we consider two types of sensing intervals, i.e., long and short intervals. In the proposed scheme, when the measured energy level exceeds v_{L} but is lower than v_{H}, the SU operates in partial-access mode, and a short sensing interval is scheduled. Otherwise, a long sensing interval is carried out, when the energy level is lower than v_{L} or higher than v_{H}.

III. Model Formulation and Analysis

Here, we analyze the proposed hybrid access strategy in the presence of imperfect spectrum sensing. A discrete-time Markov chain model is used to model the PHY layer sensing and the MAC layer access.

A. Assumptions

- For convenience, we define the long and short spectrum sensing intervals as $\Delta T_L = M\tau$ and $\Delta T_S = M'\tau$, respectively, where M and M' are positive integers. τ denotes a basic unit for the system observation interval.
- We consider the single licensed frequency channel and model the PU's access process as a two-state ON/OFF process, which specifies the time slots when the PU is active (ON) or inactive (OFF).
- At the beginning of each model observation, the probability that the PU transfers from inactive to active is λ, whereas the probability that the PU transfers from active to inactive is μ.
- When the PU becomes active, the probability that the PU appears in Region 2 is δ. It is assumed that the model observation interval is much smaller than the average PU active period. Therefore, the probability that the PU appears in two regions successively in one observation interval is negligible.

B. Model Formulation

We develop a discrete-time Markov chain model to analyze the proposed hybrid access strategy. Let $E_{(i,j)}$ and $T_{(i,j,k)}$ denote the energy detection state and the normal transmission (nonsensing) state

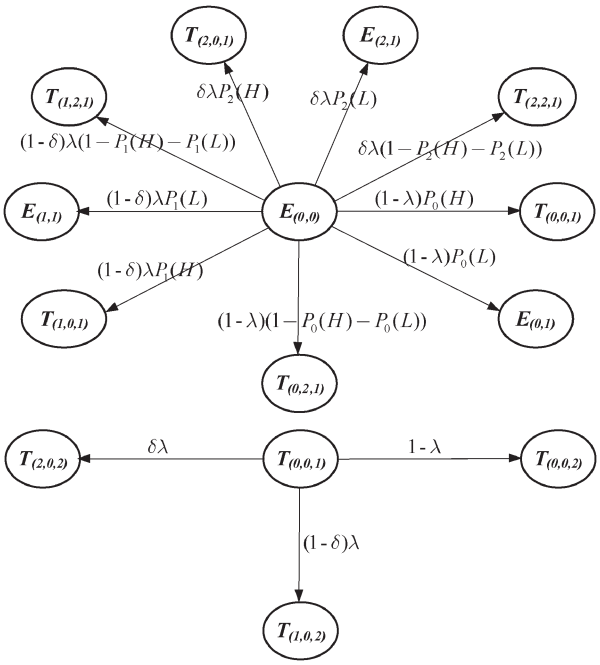

Fig. 2. Examples of the detailed state transition diagrams. (Upper) Transitions from state $E_{(i,j)}$ to $E_{(i+s,j+l)}$ and $T_{(i+s,j+l,1)}$. (Bottom) Transitions from state $T_{(i,j,k)}$ to $T_{(i+s,j,k+1)}$.

of the system model, respectively. Specifically, i indicates the status of the PU in this channel. If the PU is inactive, $i = 0$, and when the PU is in Region 1 and Region 2, $i = 1$ and $i = 2$, respectively. Additionally, j represents the access mode of the SU. If the SU is inactive, $j = 0$, and when the SU is operating in the partial- and full-access modes, $j = 1$ and $j = 2$, respectively. To make our analysis tractable, we define the short sensing interval as $\Delta T_S = \tau$. Likewise, k denotes the number of observation intervals passed during a long sensing interval ΔT_L. The state space is then given by

$$\Psi = \left\{ E_{(i,j)}, T_{(i,j,k)} \left| \begin{matrix} i,j \in \{0,1,2\} \\ k = 1,2,\ldots,M-1 \end{matrix} \right. \right\}. \tag{5}$$

Fig. 2 (upper) shows an example of state transitions from the energy detection state to the next energy detection or normal transmission state, i.e., from state $E_{(i,j)}$ to $E_{(i+s,j+l)}$ or $T_{(i+s,j+l,1)}$, where $i, i+s, j, j+l \in \{0,1,2\}$. In this case, the PU operating mode transfers from i to $i+s$, which is caused by the status changes of communicating with the PU Rx and is independent of spectrum sensing. As mentioned in the previous section, we assume that the probability that the PU appears in two regions successively in one observation interval is negligible, i.e., we do not consider the transitions from $i = 1$ to $i = 2$ or from $i = 2$ to $i = 1$ in a single observation interval τ. Hence, s can be defined as, for $i = 0$, $s \in \{0,1,2\}$; for $i = 1$, $s \in \{-1,0\}$; and for $i = 2$, $s \in \{-2,0\}$. Similarly, the SU operating mode can transfer from j to $j+l$, depending on the spectrum sensing results. For $j + l = 1$, the SU is operating in partial-access mode, and a short sensing interval is scheduled. Hence, $E_{(i,j)}$ will transfer to $E_{(i+s,j+l)}$. For $j + l \in \{0,2\}$, the SU is inactive or operating in full-access mode, and thus, a long sensing interval is scheduled. Hence, $E_{(i,j)}$ transfers to $T_{(i+s,j+l,1)}$. We further assume that energy detection is performed at the end of the transitions from $E_{(i,j)}$ to $E_{(i+s,j+l)}$ or $T_{(i+s,j+l,1)}$.

For example, in the case when both the PU and the SU are inactive, i.e., state $E_{(0,0)}$, if a PU in Region 2 starts transmitting and the measured energy level is higher than v_{H}, the system will transfer to state $T_{(2,0,1)}$, with probability $\delta\lambda P_2(\mathsf{H})$, where $P_2(\mathsf{H})$ is given by (4e). On the other hand, if the measured energy level is lower than v_{L} and the PU stays inactive, the system will transfer to state $T_{(0,2,1)}$, with probability $(1-\lambda)(1 - P_0(\mathsf{H}) - P_0(\mathsf{L}))$. For the short sensing interval case, if a PU in Region 1 starts transmitting and the measured energy level is larger than v_{L} but lower than v_{H}, the system will transfer to state $E_{(1,1)}$, with probability $(1-\delta)\lambda P_1(\mathsf{L})$.

As such, the state transition probabilities from $E_{(i,j)}$ to $E_{(i+s,j+l)}$ and $T_{(i+s,j+l,1)}$, respectively, $\gamma_1^{(i,s,j,l)}$ and $\gamma_2^{(i,s,j,l)}$, can be expressed as

$$\gamma_1^{(i,s,j,l)} = \theta_{i,s}\phi_{i,j+l}, \quad \text{for } j+l = 1 \tag{6}$$

$$\gamma_2^{(i,s,j,l)} = \theta_{i,s}\phi_{i,j+l}, \quad \text{for } j+l \in \{0,2\} \tag{7}$$

where $\theta_{i,s}$ and $\phi_{i,j}$ are the functions related to the changes of PU Tx's operating location mode and the energy detection results, which are, respectively, given by

$$\theta_{i,s} = \begin{cases} 1-\lambda, & \text{for } i=0, s=0 \\ (1-\delta)\lambda, & \text{for } i=0, s=1 \\ \delta\lambda, & \text{for } i=0, s=2 \\ (1-\mu), & \text{for } i \in \{1,2\}, s=0 \\ \mu, & \text{for } i \in \{1,2\}, s=-i \end{cases} \tag{8}$$

$$\phi_{i,j+l} = \begin{cases} P_i(\mathsf{H}), & \text{for } j+l=0 \\ P_i(\mathsf{L}), & \text{for } j+l=1 \\ 1-P_i(\mathsf{H})-P_i(\mathsf{L}), & \text{for } j+l=2 \end{cases} \tag{9}$$

where $P_i(\mathsf{H})$ and $P_i(\mathsf{L})$ can be obtained using (4a)–(4f).

Fig. 2 (bottom) shows an example of state transitions between normal transmission states, i.e., from state $T_{(i,j,k)}$ to $T_{(i+s,j,k+1)}$ during a long sensing interval, where $i, i+s \in \{0,1,2\}$, $j \in \{0,2\}$ and $1 \le k < M-1$. Since the changes of SU's operating mode only happen at the energy detection states, j will not change in this case. Therefore, to summarize the transition probabilities in this case, $\gamma_3^{(i,s)}$ is given by

$$\gamma_3^{(i,s)} = \theta_{i,s}. \tag{10}$$

For the state transitions from normal transmission states to the energy detection state, i.e., from state $T_{(i,j,M-1)}$ to $E_{(i+s,j)}$, where $i, i+s \in \{0,1,2\}$, $j \in \{0,2\}$. Similar to the given case, j will not change in such state transitions. Therefore, the transition probabilities can be defined by $\gamma_3^{(i,s)}$, which is given by

$$\gamma_4^{(i,s)} = \theta_{i,s}. \tag{11}$$

Let $\pi(E_{(i,j)})$ and $\pi(T_{(i,j,k)})$ denote the steady-state probabilities of $E_{(i,j)}$ and $T_{(i,j,k)}$, respectively. Let $\mathbf{\Pi}$ denote the row vector of steady-state probabilities with elements $\{\pi(E_{(i,j)}), \pi(T_{(i,j,k)})\}$ and $\mathbf{Y}$ denote the transition rate matrix, whose elements $\{\gamma_1^{(i,s,j,l)}, \gamma_2^{(i,s,j,l)}\gamma_3^{(i,s)}, \gamma_4^{(i,s)}\}$ can be obtained from the given analysis. Steady-state matrix $\mathbf{\Pi}$ can be obtained by solving the linear equations $\mathbf{\Pi} = \mathbf{\Pi Y}$ and $\mathbf{\Pi e} = 1$, where $\mathbf{e}$ is the column vector with all 1's.

C. Performance Analysis

Here, we derive some important performance metrics.

1) Throughput of SU: Throughput is measured by the average achievable transmission rate in bits per second (b/s). However, if the SU causes harmful interference to the PU, i.e., when the PU Rx's interference constraints are violated, the throughput achieved during these periods will not be counted. Considering sensing efficiency, we use the Shannon bound to obtain the achievable rate in a given bandwidth as

$$R = \eta W \log_2(1 + \gamma_{\mathsf{SU}}) \tag{12}$$

where γ_{SU} is the SNR of the SU, and η is the sensing efficiency, as $\eta = 1 - T_s/\Delta T$, where $\Delta T \in \{\Delta T_L, \Delta T_S\}$ and $\eta \in \{\eta_L, \eta_S\}$ correspond to the long and short sensing intervals, respectively. Let P^r_{SU} denote the average SU received power. When the PU is inactive, the SNR of the SU in this case can be calculated as

$$\overline{\gamma}_{\mathsf{SU}} = \frac{P^r_{\mathsf{SU}}}{N_0 W} \tag{13}$$

where N_0 is the one-sided noise power. On the other hand, if the PU is active in Region 1 or Region 2, the SNR of the SU in the two cases can be found as

$$\overline{\gamma}^1_{\mathsf{SU}} = \frac{P^r_{\mathsf{SU}}}{N_0 W + P^{r_1}_{\mathsf{PU}}} \quad \text{(PU in Region 1)} \tag{14}$$

$$\overline{\gamma}^2_{\mathsf{SU}} = \frac{P^r_{\mathsf{SU}}}{N_0 W + P^{r_2}_{\mathsf{PU}}} \quad \text{(PU in Region 2)} \tag{15}$$

where $P^{r_1}_{\mathsf{PU}}$ and $P^{r_2}_{\mathsf{PU}}$ are the average received PU signal power at the SU Rx in the two cases.

The average throughput of the SU can be derived as

$$\begin{aligned}\mathrm{Th} = &\sum_{i\in\{0,1,2\}} \varepsilon_i \sigma_1 \eta_S \pi(E_{(i,1)}) \\ &+ \sum_{i\in\{0,1,2\}} \sum_{j\in\{0,2\}} \sum_{1\le k\le M} \sigma_j \eta_L \left(\pi\left(E_{(i,j)}\right) + \pi\left(T_{(i,j,k)}\right)\right)\end{aligned} \tag{16}$$

where

$$\varepsilon_i = \begin{cases} R_{\mathsf{SU}}, & \text{for } i = 0 \\ R^1_{\mathsf{SU}}, & \text{for } i = 1 \\ R^2_{\mathsf{SU}}, & \text{for } i = 2 \end{cases} \tag{17}$$

in which R_{SU}, R^1_{SU}, and R^2_{SU} are the achievable rates when the SU SNRs are $\overline{\gamma}_{\mathsf{SU}}$, $\overline{\gamma}^1_{\mathsf{SU}}$, and $\overline{\gamma}^2_{\mathsf{SU}}$, respectively. In addition, interference constraint violation probability is defined as the probability that PU Rx's received power from the SU Tx exceeds its interference constraint. P^1_{ICV} and P^2_{ICV} are the average interference constraint violation probability to the PU Rx in Region 1 and Region 2, respectively, as [11, eq. (2.52)]. In addition, σ_j is the function that defines the access probability when the SU is operating in full- and partial-access modes, which is given by

$$\sigma_j = \begin{cases} 0, & \text{for } j = 0 \\ P_{\mathsf{access}}, & \text{for } j = 1 \\ 1, & \text{for } j = 2. \end{cases} \tag{18}$$

2) Interfering Probability: Interfering is said to occur when the SU causes harmful interference to the PU, i.e., when the SU miss-detects the PU's signal, and the SU's transmission power violates the interference constraints of the PU Rx. Hence, the interfering probability is given by

$$\begin{aligned}P_{\mathsf{In}} = &P^1_{\mathsf{ICV}} \sum_{j\in\{0,2\}} \sum_{1\le k\le M} \sigma_j \left[\pi(E_{(1,j)}) + \pi(T_{(1,j,k)})\right] \\ &+ P^2_{\mathsf{ICV}} \sum_{j\in\{0,2\}} \sum_{1\le k\le M} \sigma_j \left[\pi\left(E_{(2,j)}\right) + \pi(T_{(2,j,k)})\right].\end{aligned} \tag{19}$$

IV. Numerical Results

Here, we present the numerical results for evaluating the proposed hybrid access strategy, by comparing with the conventional overlay access schemes. In particular, the performance metrics of the overlay scheme can be obtained using our analytical model by using a single energy detection threshold.

A. Simulation Parameters

We set the radii of Region 1 and Region 2 as $D_1 = 300$ m and $D_2 = 100$ m, which can be referred to as the outer and inner areas of a building, respectively. Note that D_2 is an SU-defined parameter, which can be viewed as a threshold for the received PU Tx power or the size of a building. For practical network implementation, when D_2 is defined, the probability that the PU appears in Region 2, δ, can be measured. The active PU Tx and Rx are assumed to be independent and uniformly distributed in the same region (Region 1 or Region 2), respectively. In the simulations, when a PU is active, $\delta = 0.7$, and the SU Tx and Rx have fixed locations, with $d = 50$ m distance between them. We set the bandwidth of a single channel as $W = 1$ MHz and the noise power as $N_0 = -163$ dBm/Hz. In addition, we use the combined path loss and shadowing model [11] to consider the effects of path loss, shadowing, and Rayleigh fading. For PU appearing at different locations, the average received power at the SU Tx and the SU Rx can be calculated using [11, eq. (2.45)], where the parameters are defined as unitless constant $K = -31.54$, PU Tx transmission power $P^t_{\mathsf{PU}} = 13$ dBm, path loss exponent $\gamma = 3.71$, and reference distance $d_0 = 1$ m. For the double-threshold energy detection, v_{H} and v_{L} are obtained for various false-alarm probabilities 0.001 and 0.1, respectively, i.e., $v_{\mathsf{H}} = \mathcal{Q}^{-1}(0.001)$ and $v_{\mathsf{L}} = \mathcal{Q}^{-1}(0.1)$ using (1). We model shadowing using a lognormal random variable with mean zero and variance 3.65 dB, and the interference constraint to the PU is -100 dBm. Using [11, eq. (2.52)], the probability that SU's power exceeds the interference constraints at a given distance between the SU Tx and the PU Rx is found, with the SU transmission power being $P^t_{\mathsf{SU}} = 13$ dBm. We ran 10^5 independent simulations with different locations of the PU Tx and Rx, to obtain the detection probabilities in (4a)–(4f), the average received PU Tx's power at the SU Rx in (14) and (15), and the average interference constraint violation probabilities in (16).

We set the model observation interval as $\tau = 100$ ms and the time for conducting energy detection as $T_s = 50$ μs. For the sensing intervals, we set $\Delta T_L = 5\tau = 500$ ms and $\Delta T_S = \tau = 100$ ms, respectively. The probability that the PU transfers from active to inactive during a model observation is $\mu = 1/200$. If not specified otherwise, we set $\lambda = 1/600$, which corresponds to the mean PU channel utilization rate of 25%. P_{access} is set to 0.9 for the hybrid access scheme.

B. Simulation Results

Fig. 3 provides the results for the throughput of the SU and the interfering probability against the mean interarrival time of the PU. We vary the probability that the PU transfers from inactive to active at each observation interval as $1/1200 \le \lambda \le 1/100$, which corresponds to the mean PU channel utilization rate of 14.3%–66.7%. We observe that the proposed hybrid strategy achieves greater throughput than the overlay schemes with the single detection threshold v_{L}. In contrast to this overlay scheme, the SU in the hybrid strategy can share the channel with the active PU via the partial-access mode, in which the SU will less likely cause harmful interference to the PU. It is also observed that the hybrid strategy achieves a much lower interfering probability than the overlay scheme with v_{H}. The reason is that the double-threshold energy detection scheme can provide the false alarm–detection performance tradeoff to near-side and far-end PUs by arranging the long and short sensing intervals. Furthermore, the performance gain over overlay schemes is more noticeable when there

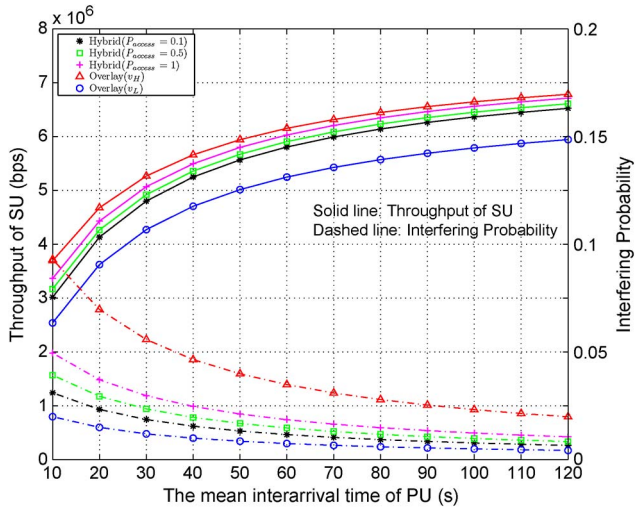

Fig. 3. Throughput of the SU and the interfering probability against the mean interarrival time of the PU.

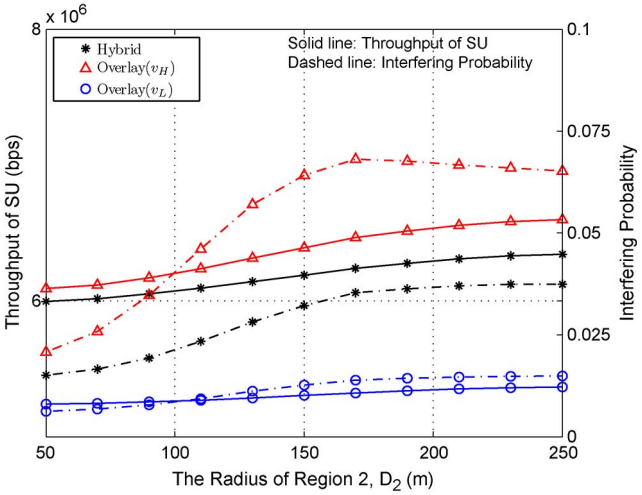

Fig. 4. Throughput of the SU and the interfering probability against the radius of Region 2.

is a lower mean interarrival time of the PU, i.e., a higher PU channel utilization rate. In particular, the hybrid strategy with $P_{\text{access}} = 1$ can achieve 46.86% improvement on interfering performance, at the cost of 1.28% decrease in throughput, as compared with the overlay scheme with v_{H}. By adjusting partial-access probability P_{access}, a tradeoff between throughput and interfering probability can be adjusted, following the system quality-of-service requirements.

In Fig. 4, we study the impact of the radius of Region 2 D_2. With a larger value of D_2, the average interference constraint violation probability in Region 1 and Region 2 decreases. As a result, a larger throughput can be achieved. On the other hand, in this case, the interfering probability first increases with D_2 and then decreases in all three hybrid and overlay access schemes. This can be explained by recognizing the fact that the interfering probability is jointly determined by the miss-detection probability and the average interference constraint violation probability. With increasing D_2, the SU has a greater chance to miss-detect the PU Tx's signal, which results in the increase in the miss-detection probability. However, although the SU may miss-detect PU Tx's signal and start transmission, it is less likely that the transmission will cause harmful interference to the PU, due to a lower PU's interference constraint violation probability.

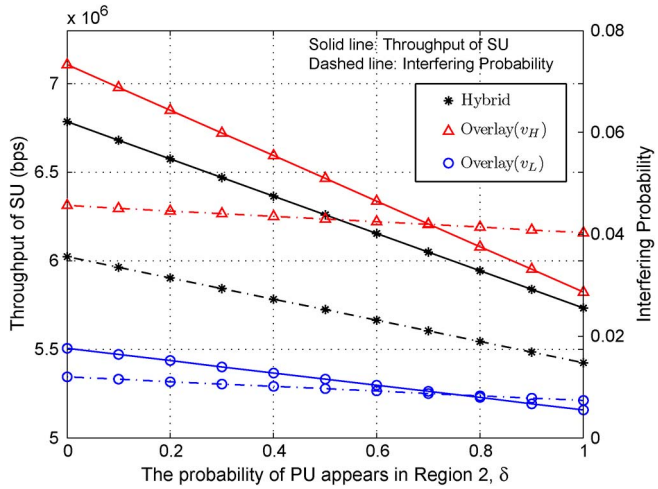

Fig. 5. Throughput of the SU and the interfering probability against the probability that the PU appears in Region 2.

Fig. 5 shows the effect of the probability that the PU appears in Region 2 δ. We see that with a larger probability that the PU appears in the near-side, both interfering and throughput decrease for the proposed hybrid strategy. Due to the lower average miss-detection probability in Region 2, if more PUs appear, there will be less chance that the PU will be interfered. On the other hand, it is more likely that the SU stays inactive rather than operates in partial-access mode, and therefore, a lower throughput can be observed as expected.

V. Conclusion

This correspondence has proposed and analyzed a new hybrid access strategy for DSA. A CR-based double-threshold energy detection method was employed to identify the PU's location. Spectrum sensing at the PHY layer and users' access process at the MAC layer were jointly modeled by a discrete-time Markov chain. Numerical results revealed that the hybrid strategy can achieve 46.86% improvement on interfering probability, as compared with the conventional overlay scheme. Moreover, SUs can adjust the access probability of partial-access mode and coordinate the long and short sensing intervals to achieve a better tradeoff between throughput and interfering performance. In future works, we will develop a general analytical model by considering the various number of PUs and SUs and multiple number of sharing channels, with the cross-layer optimization framework on parameters such as sensing interval, sensing time, partial-access probability, etc.

References

[1] Q. Zhao and B. M. Sadler, "A survey of dynamic spectrum access," *IEEE Signal Process. Mag.*, vol. 24, no. 3, pp. 79–89, May 2007.
[2] J. Mitola, "Cognitive radio for flexible mobile multimedia communications," *Mobile Netw. App.*, vol. 6, no. 5, pp. 435–441, Sep. 2001.
[3] A. Ghasemi and E. S. Sousa, "Spectrum sensing in cognitive radio networks: The cooperation–processing tradeoff," *Wireless Commun. Mobile Comput.*, vol. 7, no. 9, pp. 1049–1060, Nov. 2007.
[4] T. Cui, F. Gao, and A. Nallanathan, "Optimization of cooperative spectrum sensing in cognitive radio," *IEEE Trans. Veh. Technol.*, vol. 60, no. 4, pp. 1578–1589, May 2011.
[5] Y.-C. Liang, Y. Zeng, E. C. Y. Peh, and A. T. Hoang, "Sensing–throughput tradeoff for cognitive radio networks," *IEEE Trans. Wireless Commun.*, vol. 7, no. 4, pp. 1326–1337, Apr. 2008.
[6] X. Kang, R. Zhang, Y.-C. Liang, and H. K. Garg, "Optimal power allocation strategies for fading cognitive radio channels with primary user outage constraint," *IEEE J. Sel. Areas Commun.*, vol. 29, no. 2, pp. 374–383, Feb. 2011.

[7] S. Stotas and A. Nallanathan, "Optimal sensing time and power allocation in multiband cognitive radio networks," *IEEE Trans. Commun.*, vol. 59, no. 1, pp. 226–235, Jan. 2011.
[8] J. Oh and W. Choi, "A hybrid cognitive radio system: A combination of underlay and overlay approaches," in *Proc. IEEE Veh. Technol. Conf.*, Ottawa, ON, Canada, Sep. 6–9, 2010, pp. 1–5.
[9] V. Chakravarthy, X. Li, Z. Wu, M. Temple, F. Garber, R. Kannan, and A. Vasilakos, "Novel overlay/underlay cognitive radio waveforms using SD-SMSE framework to enhance spectrum efficiency—part I: Theoretical framework and analysis in AWGN channel," *IEEE Trans. Commun.*, vol. 57, no. 12, pp. 3794–3804, Dec. 2009.
[10] M. G. Khoshkholgh, K. Navaie, and H. Yanikomeroglu, "Access strategies for spectrum sharing in fading environment: Overlay, underlay, and mixed," *IEEE Trans. Mob. Comput.*, vol. 9, no. 12, pp. 1780–1793, Dec. 2010.
[11] A. Goldsmith, *Wireless Communications*. Cambridge, U.K.: Cambridge Univ. Press, 2005.

SINR Distribution for MIMO MMSE Receivers in Transmit-Correlated Rayleigh Channels: SER Performance and High-SNR Power Allocation

Wonsop Kim, *Student Member, IEEE*, Namshik Kim, Hyun Kyu Chung, and Hyuckjae Lee, *Member, IEEE*

***Abstract*—In this paper, a multiple-input–multiple-output (MIMO) system with a precoder is considered in transmit-correlated Rayleigh channels. We specifically target the MIMO system employing minimum-mean-square-error (MMSE) receivers. Based on the random matrix theory, we first present a direct and generalized formulation for deriving a probability density function (pdf) of the signal-to-interference-plus-noise ratio (SINR). Then, we derive accurate closed-form SINR pdfs for a small number of transmit and receive antennas. Based on the SINR pdfs, tight closed-form approximations of the symbol error rate (SER) are derived. In the high-signal-to-noise-ratio (SNR) regime, we also propose high-SNR power allocation (HPA) by minimizing the modified global SER approximation. At high SNRs, the computationally efficient HPA performing similar to optimal power allocation (PA) shows noticeable performance gain over the equal PA, particularly at the high transmit correlation. Moreover, the performance gain of the proposed HPA increases with the diversity order.**

***Index Terms*—Correlated channels, minimum mean square error (MMSE), multiple-input multiple-output (MIMO), signal-to-interference-plus-noise ratio (SINR), symbol error rate (SER).**

Manuscript received July 11, 2012; revised November 18, 2012 and March 3, 2013; accepted April 25, 2013. Date of publication May 17, 2013; date of current version October 12, 2013. This work was supported in part by the Korea Communications Commission through the R&D program supervised by the Korea Communications Agency under Grant KCA-2012-(12-911-01-105) and in part by the Ministry of Science, ICT and Future Planning, Korea, through its IT R&D programs (Research on Advanced Technologies of Access Network for Traffic Capacity Enhancement, 13ZI1120). The review of this paper was coordinated by Dr. A. J. Al-Dweik.

W. Kim is with the Precision Guidance Technology Center, Agency for Defense Development, Daejeon, Korea (e-mail: topsop@add.re.kr).

N. Kim and H. Lee are with the Department of Electrical Engineering, Korea Advanced Institute of Science and Technology, Daejeon, Korea (e-mail: nskim@kaist.ac.kr; hjlee314@kaist.ac.kr).

H. K. Chung is with the Mobile Telecommunication Research Laboratory, Electronics and Telecommunications Research Institute, Daejeon, Korea (e-mail: hkchung@etri.re.kr).

Color versions of one or more of the figures in this paper are available online at http://ieeexplore.ieee.org.

Digital Object Identifier 10.1109/TVT.2013.2263157

I. Introduction

Multiple-input–multiple-output (MIMO) communication has been considered to be a promising technique due to its potential in improving system reliability and capacity [1]. Diversity gain improves link reliability, whereas spatial multiplexing (SM) gain increases the data rate. In this paper, we focus on the SM systems with a minimum-mean-square-error (MMSE) receiver [2] only.

The transmitted signal of MIMO MMSE receivers may be optimized with a precoder [3]–[7]. In [3] and [4] perfect channel state information (CSI) is assumed at both the transmitter and the receiver. In [5]–[7], transmit (Tx) and receive (Rx) correlation matrices are available at the transmitter only. It was shown in [5]–[7] that, under various criteria (e.g., MMSE and maximum ergodic capacity), the left eigenvectors of the optimal precoder coincide with the eigenvectors of the Tx correlation matrix.

The probability density function (pdf) of the signal-to-interference-plus-noise ratio (SINR) and the symbol error rate (SER) for MIMO MMSE receivers in uncorrelated Rayleigh channels were derived in [2] for a small number of N_t Tx and N_r Rx antennas. The SER for diversity-combining MMSE receivers in the transmit-correlated Rayleigh channels was analyzed in [8].[1] However, [8] did not deal with the SINR pdf and power allocation (PA) over the Tx antennas. For the transmit-correlated Rayleigh channels, it was found in [9] that the SINR for the MMSE receivers approaches a Gamma or a generalized Gamma. Using both distributions [9], the approximated bit error rate (BER) was analyzed in [6]. However, [6] showed the limits on accuracy imposed by approximated distributions.

This paper considers MIMO MMSE receivers with precoding in the transmit-correlated Rayleigh channels. We assume that perfect CSI is known at the receiver but that only its Tx and Rx correlation matrices are available at the transmitter. Based on the random matrix theory, we first provide a generalized formulation for deriving the SINR pdfs without assuming the approximated distributions. For small N_t and N_r, we derive the closed-form SINR pdfs. Using the SINR pdfs and a close approximation [2] of the Gaussian Q-function, we derive tight closed-form SER approximations. Our analysis shows that both the derived SERs and Monte Carlo (MC) simulations have almost identical results, whereas the expressions obtained in [6] show substantial mismatches.

The PA that minimizes the outage probability subject to the total power constraint has been widely studied in the literature [10], [11]. We show that, at high signal-to-noise ratios (SNRs), the global SER approximation is strictly convex with respect to the Tx power ratio. Using a convex optimization framework, we propose high-SNR PA (HPA) with the aim of minimizing the modified global SER approximation. At high SNRs, computationally efficient HPA performing similiar to optimal PA (i.e., an exhaustive search at all SNRs) outperforms equal PA. The closed-form SERs and HPA can be used to optimize practical system designs, since one could compute them efficiently.

II. System Model

Let us consider a point-to-point MIMO system with N_t Tx and N_r Rx antennas ($N_r \geq N_t$). We focus on an SM system where the N_t streams are mapped to Gray-coded M-ary quadrature amplitude

[1] Note that the transmit-correlated channel scenario typically occurs when a small mobile station with closely spaced antennas communicates with a base station with widely spaced antennas [13].